A Patterned 3D Silicon Anode Fabricated by Electrodeposition on a Virus-Structured Current Collector

Xilin Chen, Konstantinos Gerasopoulos, Juchen Guo, Adam Brown, Chunsheng Wang, Reza Ghodssi, and James N. Culver*

Electrochemical methods were developed for the deposition of nanosilicon onto a 3D virus-structured nickel current collector. This nickel current collector is composed of self-assembled nanowire-like rods of genetically modified tobacco mosaic virus (TMV1cys), chemically coated in nickel to create a complex high surface area conductive substrate. The electrochemically deposited 3D silicon anodes demonstrate outstanding rate performance, cycling stability, and rate capability. Electrodeposition thus provides a unique means of fabricating silicon anode materials on complex substrates at low cost.

1. Introduction

Silicon is a promising anode material for next-generation high-capacity lithium-ion batteries because of its high theroretical capacity (3572 mAh g^{-1}[1,2]) and low charge/discharge voltage at room temperature. However, silicon experiences a large volume expansion during lithium ion insertion and a corresponding shrinkage during lithium ion extraction. This large volume change leads to severe silicon particle pulverization, loss of contact with the current collector, and subsequent electrode failure.[3,4]

The pulverization of silicon particles can be alleviated by reducing the particle size and introducing nanopores into silicon. Silicon nanowires, nanotubes and porous silicon have all demonstrated improved electrochemical performance.[4–12] These nanofiber and nanoporous structures can volumetrically accommodate the expansion that occurs upon lithium insertion and are thus resistant to subsequent structural failure.[11,12]

Dr. X. Chen, Dr. J. Guo, Prof. C. Wang
Department of Chemical and Biomolecular Engineering
University of Maryland College Park
MD 20742, USA
E-mail: cswang@umd.edu
K. Gerasopoulos, Prof. R. Ghodssi
Department of Materials Science and Engineering
Institute for Systems Research
Department of Electrical and Computer Engineering
University of Maryland College Park
MD 20742, USA
A. Brown, Prof. J. N. Culver
Institute for Bioscience and Biotechology Research
Department of Plant Science and Landscape Architecture University of Maryland College Park
MD 20742, USA

DOI: 10.1002/adfm.201001475

Currently, silicon nanowires and nanotubes are fabricated using chemical vapor deposition (CVD)[4,12,13] and wet chemical methods.[11] However, CVD technology is based on expensive and complex equipment and cannot uniformly deposit silicon onto a complex 3D substrate; at the same time, the wet chemical silicon deposition is a very complicated and time-consuming procedure. In this work, an electrodeposition method was employed to deposit silicon and improve the uniformity of the deposition on the 3D tobacco mosaic virus/nickel (TMV1cys/Ni) current collector. In electrodesposition, the silicon is deposited from organic solvents using SiX_4 or $SiHX_3$ (X = Cl, Br) as solutes.[14–19] When $SiCl_4$ is used as a solute, it is electrochemically reduced to form silicon by the following reactions:

$$SiCl_4 + 4e^- = Si + 4Cl^- \text{(working electrode)} \quad (1)$$

$$4Cl^- = 2Cl_2 + 4e^- \text{(counter electrode)} \quad (2)$$

Even though electrodeposition is a simple and low-cost method that can uniformly deposit silicon thin-films onto various metal substrates,[14–19] it has not been used to-date to fabricate silicon anodes for lithium-ion batteries.

Since silicon is a semiconductor, carbon nanofiber cores or carbon coatings are normally used to improve the electronic conductivity of silicon nanowires. Carbon–silicon core–shell nanowires[8] have a better rate capability than silicon nanowires.[4] However, these carbon nanofibers were not patterned on a substrate nor were they directly connected to the current collector as was done for the patterned silicon nanowires[4] and silicon nanotubes.[12] Carbon nanofiber conductivity is also not as good as that of metals. In our work, a 3D current collector (**Figure 1**a), self-assembled and composed of nickel-coated genetically modified TMV1cys,[13,20–23] is used as a current collector to electrochemically deposit silicon nanowire anodes for lithium-ion batteries that each contain an individual nickel core as a current collector (Figure 1b). Unlike previously reported methodologies using biological templates for the synthesis of nanomaterials that require powder mixing and ink-casting for electrode fabrication,[24] the method presented in this study involves the direct fabrication of a nanostructured silicon electrode. Both the powder mixing process and binders are not needed. Different from the arrayed silicon nanotubes,[12] the nickel-core silicon-shell nanowires described in this paper

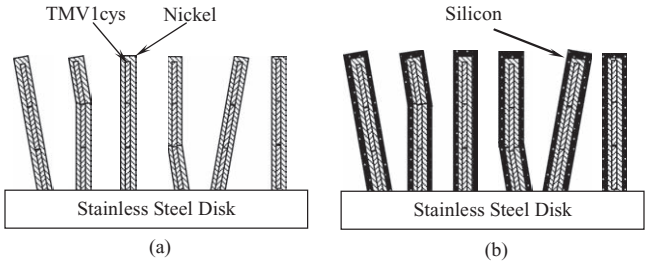

Figure 1. Diagram of a) a patterned 3D TMV1cys/Ni current collector and b) 3D silicon anode.

provide robust integration and high electronic conductivity throughout the silicon nanowire.

2. Results and Discussion

2.1. 3D TMV1cys/Ni Current Collector

Figure 2 shows the image of a nickel-coated TMV1cys current collector. TMV1cys/Ni core–shell nanowires are near-vertically patterned on the steel disk surface to form 3D current collectors, thus providing a highly electron conductive path for every silicon nanowire, as discussed later. TMV1cys was genetically modified to display a unique cysteine residue on the outer surface of each of the ≈2100 coat protein subunits that make up a rod-shaped TMV particle.[20] The strong and covalent-like interactions between the thiol groups of the engineered coat-protein cysteines and the metal ions[23] produces a strong bond between the virus template and the stainless steel substrate surfaces as well as the nickel coating layer, thus forming a robust, patterned 3D nickel current collector. In addition, the position and surface accessibility of the 1cys modification direct the surface assembly of the virus through the 3' end of the TMV rod, directing the virus to self-assemble in a vertically oriented manner. Nickel coatings of surface assembled viruses utilize a room-temperature-based electroless plating method.[20] The thickness of the nickel coating layer was ≈50 nm, as shown in Figure 2. The final length of the nickel nanowires was about 650 nm ± 300 nm due to the self-alignment of two or three TMV1cys virus particles.[13] As also shown in Figure 1,2, some nickel-coated TMV1cys rods are not vertical because of the surface roughness of the substrate and the flexibility of the attachment between two TMV1cys particles or TMV1cys and the substrate.[13] The integrity of the nickel with the stainless steel substrate makes an excellent current collector with a unique patterned 3D structure. Both the self-assembly of the virus surfaces and subsequent nickel coatings are comparably simple bench top processes that do not require specialized equipment or processing.

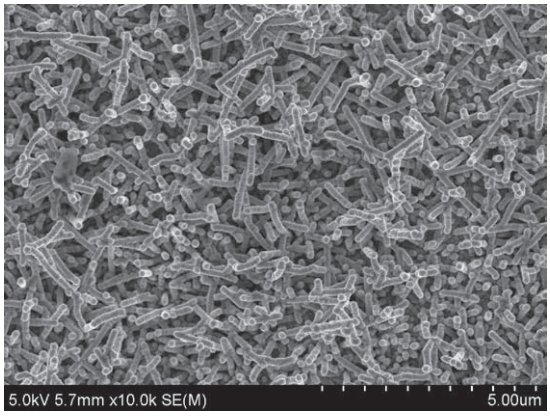

Figure 2. Scanning electron microscopy (SEM) image of the prepared 3D TMV1cys/Ni current collector.

2.2. Electrodeposition of Silicon on the TMV1cys/Ni Current Collector from $SiCl_4$

Prior to the silicon plating, the deposition potential of silicon on the TMV1cys/Ni current collector was determined using linear polarization in a custom-made cell (**Figure 3**a). In this setup, only the side with TMV1cys/Ni coating was facing the electrolyte, while platinum foil and a platinum wire were used as the counter electrode (CE) and the quasi reference electrode (QRE), respectively. Figure 3b shows a linear polarization curve for the TMV1cys/Ni substrate in propylene carbonate (PC) containing tetrabutylammonium chloride (TBACl, 0.1 M) with $SiCl_4$ (0.5 M). A cathodic peak at –2.33 V vs the Pt QRE was observed in Figure 3b. This current peak was attributed to $SiCl_4$ reduction by Munisamy et al.[19] and Agrawal et al.[24] To validate the silicon electrodeposition potential at –2.33 V, chronoamperometry and chronopotentiometry techniques were employed in the same cell. As shown in **Figure 4**a, the chronopotentiogram at a constant current density of –1.0 mA cm^{-2} shows a reduction potential plateau at –2.2 V vs Pt QRE, confirming the silicon electrodeposition from $SiCl_4$ solution at around –2.2 V. The slight shift of the reduction potential in the chronopotentiogram towards more negative potentials after ≈2500 s is probably attributed to the increase in resistance due to growth of the semiconducting silicon layer. In Figure 4b, the chronoamperogram at a reduction potential of –2.4 V vs Pt QRE shows a current density plateau at –1.2 mA cm^{-2}. The shift of the reduction current density in the chronoamperogram towards less negative currents after an equal time interval of ≈2500 s is also attributed to the aforementioned increase in resistance. During chronoamperometric and chronopotentiometric deposition of silicon, the black TMV1cys/Ni substrate turned light green, indicating the deposition of silicon. The light-green layer was confirmed to be silicon by transmission electron microscopy (TEM) and energy dispersive X-ray spectroscopy (EDS). All chronoamperogram, chronopotentiogram, and linear polarization measurements demonstrated that silicon can be electrochemically deposited on TMV1cys/Ni substrates at approximately –2.2 to –2.3 V. Based on these preliminary experiments, a potential of –2.4 V was used to deposit silicon on the TMV1cys/Ni substrate to achieve a smooth silicon coating layer.

2.3. Determination of Specific Capacity

Since the less dense electrodeposited silicon is highly sensitive to oxygen, it is very difficult to accurately measure the

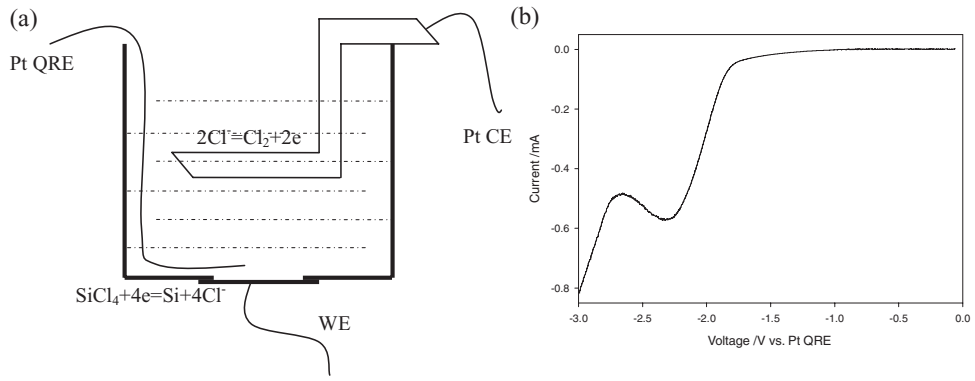

Figure 3. a) Diagram of the cell for electrodeposition and b) linear polarization for the TMV1cys/Ni current collector in $SiCl_4$–TBACl–PC electrolyte.

silicon weight without exposing the deposited silicon film to air. Also, the amount of electrodeposited silicon cannot simply be calculated by Faraday's law, due to side reactions during the electrodeposition process, i.e., the efficiency of the electrodeposition is less than 1. If the efficiency (η) of silicon electrodeposition on the 3D TMV1cys/Ni substrate is a constant, the first lithium extraction capacity should linearly increase with silicon deposition capacity. Here, the first lithium extraction capacity rather than the first lithium insertion capacity is used to avoid the effect of solid electrolyte interphase (SEI) film capacity.

Assuming the efficiency of electrochemical deposition is η, the moles (n) of deposited silicon based on the reaction (Equation 1) can be calculated from the deposition capacity Q

$$n = \eta\frac{3.6\times Q}{4\times F} \tag{3}$$

Here, F is the Faraday constant, Q is the consumed electrical charge during silicon electrodeposition in mAh, and 3.6 is a constant generated by the unit different between Q and F.

Assuming one mole of silicon atom alloys with x mole of lithium atoms in 3D TMV1cys/Ni/Si,

$$\mathrm{Si} + x\mathrm{Li}^+ + x\mathrm{e}^- = \mathrm{Li}_x\mathrm{Si} \tag{4}$$

The lithium extraction capacity from m mole of deposited silicon can be calculated by

$$C = \frac{x\times F\times n}{3.6} \tag{5}$$

Here, C is the first lithium extraction capacity from silicon in mAh and 3.6 is a constant generated by the unit different between C and F.

Combining Equation 3 and 5, the relationship between the first lithium extraction capacity (C) and silicon deposition capacity (Q) can be obtained:

$$C = \eta\frac{x\times Q}{4} \tag{6}$$

Figure 5 shows the linear relationship between C and Q. The fitted line has a slope of 0.22. Therefore, the specific capacity (x) of Li extraction from silicon can be determined using Equation 7 if the efficiency (η) of the silicon deposition is known.

$$x = \frac{0.88}{\eta} \tag{7}$$

Gobet et al.[16] reported that the average efficiency of electrochemical silicon deposition in $SiCl_4$ solution is ≈35%. Since the

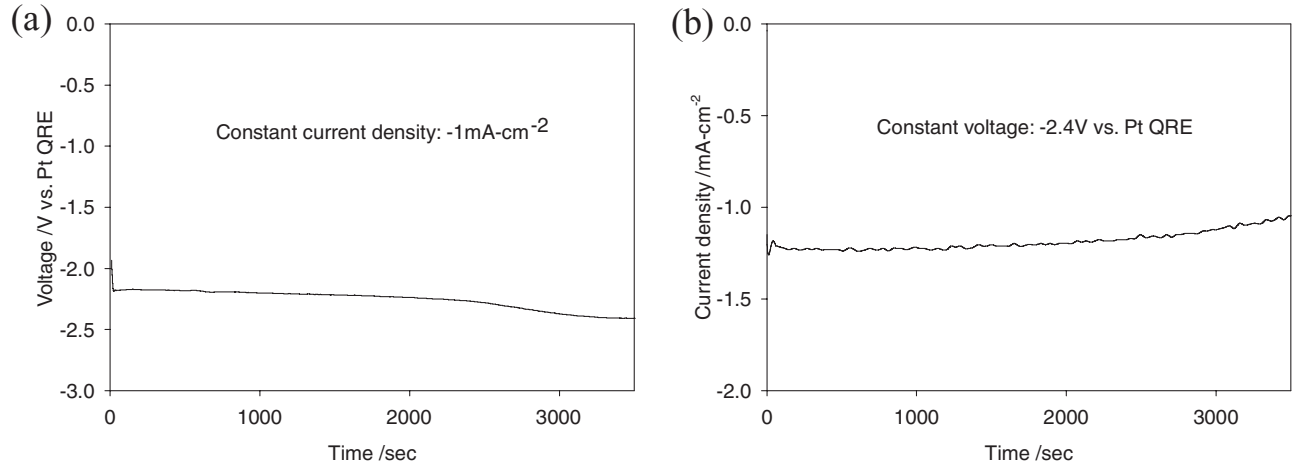

Figure 4. a) Chronopotentiogram (current density: –1 mA cm^{-2}) and b) chronoamperogram (voltage: –2.4 V vs Pt QRE) for TMV1cys/Ni current collector in $SiCl_4$-TBACl-PC electrolyte.

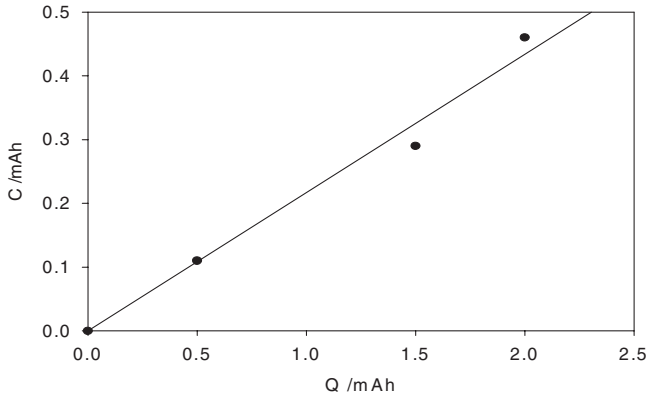

Figure 5. Initial lithium insertion capacity (*C*) of the silicon vs silicon deposition capacity (*Q*).

electrolyte and deposition parameters used in this work are similar to those in Gobet's work, an efficiency of 35% is also used to calculate the lithium extraction capacity $x = 2.51$. The first lithium extraction capacity calculated from $x = 2.51$ is 2400 mAh g^{-1}.

The TMV1cys/Ni/Si sample prepared by electrochemical deposition at −2.4 V with a cut-off charge of 2 mAh was used as a typical electrode for lithium insertion/extraction tests and characterization.

2.4. Characterization of Electrochemically Deposited Silicon

After silicon deposition on a TMV1cys/Ni substrate at −2.4 V for 2 mAh, an 80-nm silicon layer was uniformly electrodeposited onto the virus-assembled nickel surface, as shown in **Figure 6**. The electrodeposited silicon layer appears transparent and the virus-templated nickel cores are visible in the SEM image, demonstrating that the electrodeposited silicon from non-aqueous solutions has a lower density and porous structure. This result is consistent with previous findings reported in the literature.[18] Interestingly, the silicon layer prepared by physical vapor deposition (PVD)[13] is not transparent under the same SEM parameters. This phenomenon indicates that the silicon layer prepared by electrodeposition in liquid solution is less dense than that prepared by PVD in gas. The prepared anode has a core–shell structure with three layers: TMV1cys, templated nickel, and electrodeposited silicon, as show in Figure 6b. The EDS data shown in Figure 6c,d reveal the distribution of these elements in cross section. A noticeable decrease in intensity at the center of each templated nanowire is attributed to the TMV1cys. EDS analysis also revealed the presence of oxygen (data not shown). The oxygen was likely derived from air exposure[16–19] during transfer from the glove box to the TEM chamber for EDS analysis. The ratio of oxygen and silicon was about 1.6 based on quantitative EDS analysis, which is 2.4 times higher than the oxygen levels observed upon silicon sputtering.[13] The high oxygen content present in electrodeposited silicon may be attributed to a less dense silicon structure, which would allow rapid oxidation throughout the silicon layer. To avoid oxidation, silicon electrodeposition, heat treatment, carbon coating, and coin cell assembly were conducted in an argon-filled glove box.

2.5. Li Insertion/Extraction During Cyclic Voltametry Scans

Figure 7 shows the lithium insertion/extraction cyclic voltametry (CV) curve of a TMV1cys/Ni/Si electrode in a coin cell. During the first discharge (lithium insertion) only one reduction peak near 0.0 V is observed, which is a typical characteristic of crystalline silicon. However, the first charge (lithium extraction) curve shows two oxidation peaks at 0.3 and 0.5 V, while in the following discharge–charge processes, two reduction and oxidation peaks are observed; the presence of these peaks indicates a conversion from crystal silicon to amorphous silicon during charge/discharge cycling. As a consequence of the conversion of crystalline to amorphous silicon in the second and third charge and discharge cycles, the intensity of the first reduction peak increases while the intensity of the second peaks decreases. In

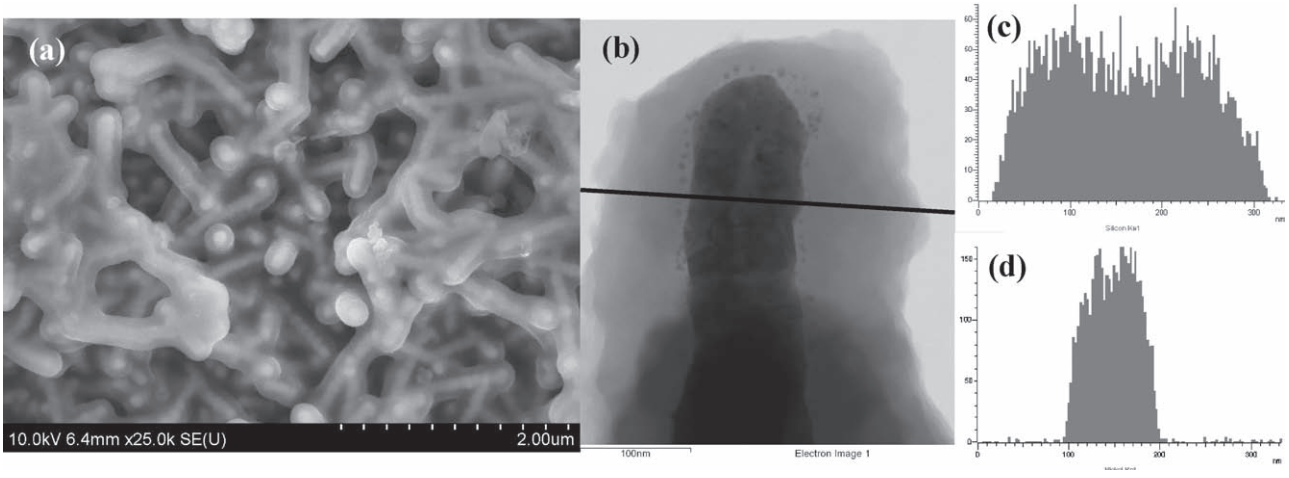

Figure 6. a) SEM image of the prepared 3D silicon anode and b) TEM image of a single nickel-silicon core–shell nanowire. c) The distribution of silicon along the radical direction and d) the distribution of nickel along the radical direction.

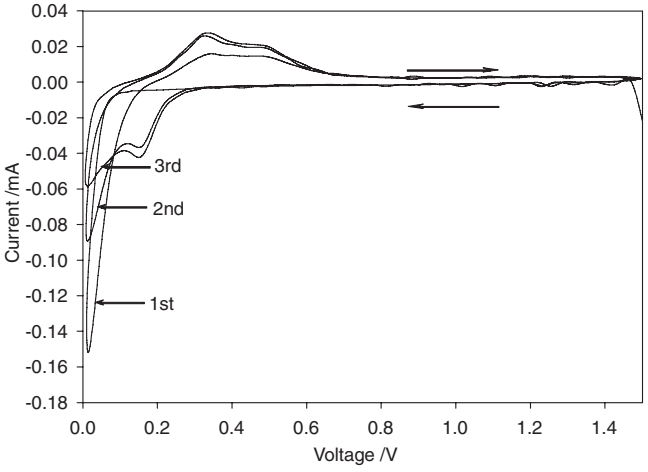

Figure 7. Cyclic voltametry of a half cell using the prepared silicon as the working electrode and lithium metal as the counter electrode.

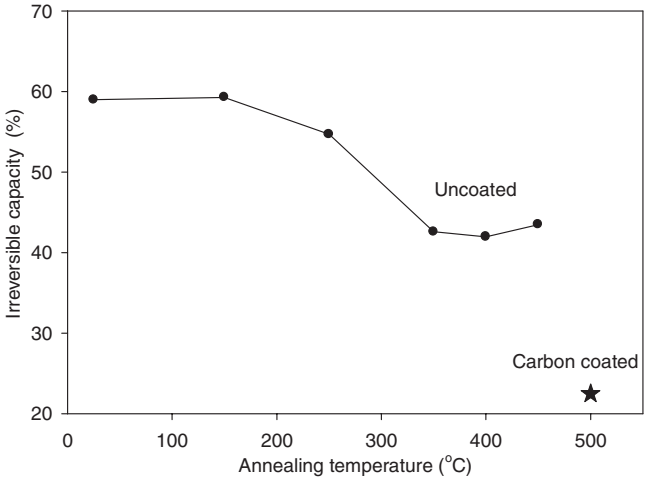

Figure 8. Irreversible capacities as a function of annealing temperatures.

addition, the intensity of the two oxidation peaks also slightly increases with repeated cycling, corresponding to the lithium-ion extraction from the amorphous silicon.[26] This behavior is consistent with the reported CV curves for crystalline silicon[4,25,26] and demonstrates that the electrochemically deposited silicon film has crystal structure. Since the electrodeposited silicon is extremely active and was oxidized immediately upon exposure to the air[16–19] during transfer from the glove box to TEM, SEM, or X-ray diffraction (XRD) apparatuses, we were unable to directly identify the crystalline nature of the electrodeposited film.

2.6. Irreversible Capacity and Charge/Discharge Behavior

The patterned 3D silicon anodes showed very high irreversible capacity (60%) in the first charge/discharge cycle. Both the porous structure of the electrodeposited silicon and the impurities generated during electrodeposition, as well as those introduced during nickel electroless deposition onto the TMV1cys template, likely contribute to the observed large irreversible capacity. The impurities introduced during electrochemical silicon deposition can be Si_xO with traces of metal, C, Cl, and $Si–H_2$ or Si–H impurities in PC solvent.[14,17] Annealing under argon can partially remove the impurities, thus improving the quality of the deposited silicon.[19] To remove impurities, the raw electrodeposited silicon was heated to 150, 250, 350, 400, 450, and 500 °C in an argon-filled glove box for 1 h. As shown in **Figure 8**, the irreversible capacity decreases with increasing temperature and levels off to a minimum value of 42.6% at 350 °C or greater. Since carbon coatings on silicon can stabilize the SEI film, decreasing the irreversible capacity and improving the columbic efficiency,[27] a layer of carbon was added to the electrodeposited silicon by coating and carbonizing polyacrylonitrile (PAN) at 500 °C in argon for 1 h. This carbon coating significantly reduced the irreversible capacity to 22.5%, as demonstrated in Figure 8.

2.7. Cyclic Stability

The cyclic performance of the patterned 3D TMV1cys/Ni/Si anode at 0.25 C is shown in **Figure 9**a. The electrodeposited

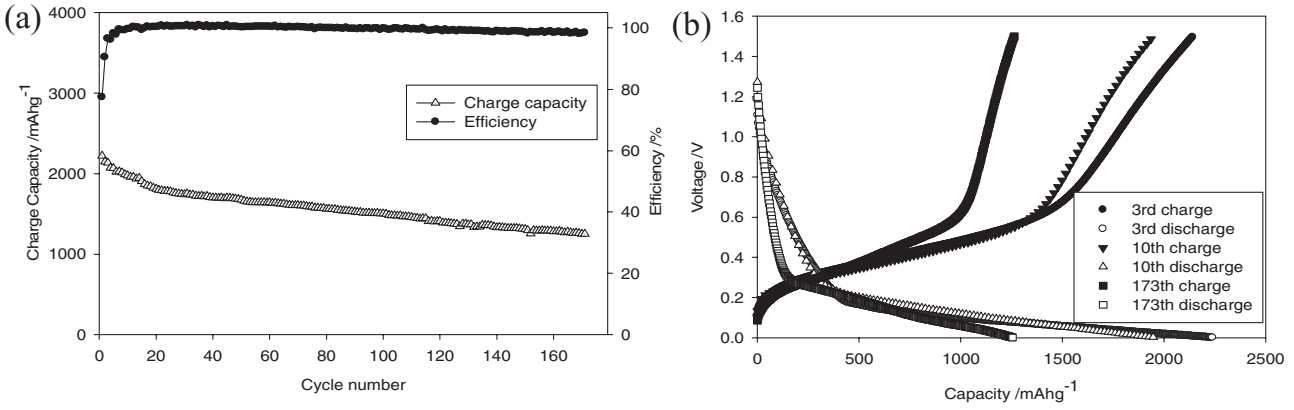

Figure 9. Cyclic stability of the coin cell (a) and charge/discharge curves (b) of a coin cell using the prepared silicon as the working electrode and lithium metal as the counter electrode.

silicon demonstrates a high reversible capacity (2300 mAh g^{-1}). The columbic efficiency rapidly increases from 77.5% in the first cycle to 99.5% in the 8th cycle. Even after 173 cycles, the capacity of the anode is retained at 1200 mAh g^{-1}, which is nearly three times that of current commercial graphite anode materials (372 mAh g^{-1}). The capacity decrease per cycle is only ≈0.25%, which is more stable than previously reported silicon nanotubes.[12] The superior capacity retention and columbic efficiency of TMV1cys/Ni/Si architecture demonstrated that the robust nickel core inside each silicon nanowire can greatly improve the structural integrity and conductivity of the anode. In addition, the high electronic conductivity of nickel and the large contact area between silicon and nickel in the TMV1cys/Ni/Si structure allow for both uniform lithium insertion and extraction within the silicon and stress reduction on the silicon nanowires. The voltage profiles in the third, 70th, and 173th charge/discharge cycles are shown in Figure 9b.

To investigate degradation mechanisms of the TMV1cys-structured nanowires, the silicon anode structure was examined after 70 cycles. Prior to disassembling the coin cell, a constant voltage of 1.5 V was applied to the silicon electrodes for a period of 48 h to completely extract lithium from the silicon. Shown in **Figure 10** are SEM images after 70 cycles of operation in different magnifications. As shown in Figure 6a and Figure 10, no obvious morphology changes can be observed after 70 charge/discharge cycles. Thus, the loose silicon shell and the mechanical integrity between silicon, nickel, and the surface-attached virus were highly resistant to the stresses associated with silicon expansion. Therefore, the structure of the electrodeposited silicon combined with the mechanical integrity of the TMV1cys/Ni/Si surface likely accounts for the observed cycling stability.

Figure 11 shows the impedances of the patterned electrodeposited silicon on a TMV1cys/Ni current collector after different cycles. The impedances were measured upon reaching a full charge. All the impedance spectra have similar features: a medium-to-high frequency depressed semicircle and an inclined low frequency line, a behavior that is in good agreement with previously reported impedance spectra of silicon nanowires.[7] The inclined line in the low-frequency region represents the lithium diffusion impedance,[28] while the depressed semicircle is attributed to the overlap between the SEI film and the interfacial charge transfer impedance.[7] Impedance studies revealed that the total SEI and charge transfer resistances increase at first and then decrease after the 3rd cycle, although the capacity continuously decreases during the charge/discharge cycles. The improved kinetics of the charge/discharge cycles may be attributed to increasing silicon porosity during repeated lithium insertion and extraction[29] and to enhanced electronic conductivity due to trapped lithium in the silicon layer.

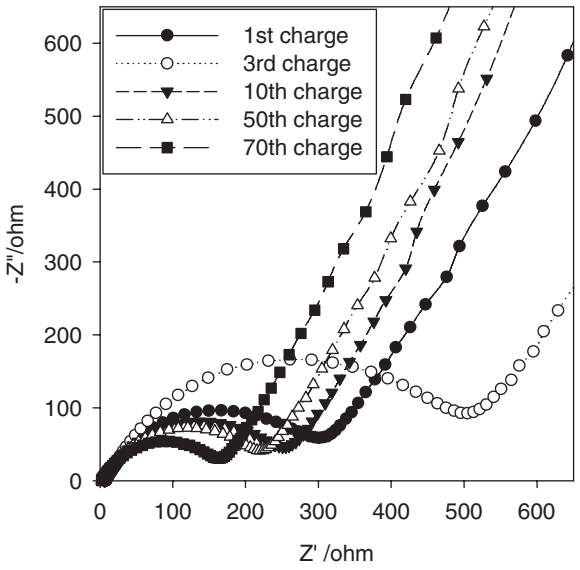

Figure 11. Impedance study of the electrodeposited silicon anode.

2.8. Rate Performance

The unique 3D substrate structure, the high electronic conductivity, and the integrity of the nickel core and silicon shell in the electrodeposited silicon anode are assumed to benefit the rate capability of the electrodeposited silicon. To verify this assumption, a half battery using electrodeposited silicon as a working electrode and lithium foil as counter electrode was tested at various *C*-rates to investigate the rate capacity. At each *C*-rate, the battery was tested for 20 cycles to ensure the reliability of the reported readings. As shown in **Figure 12**, the electrodeposited silicon shows an average charge capacity of 1818, 1504, 1370, 1202, and 985 mAh g^{-1} at 0.25, 0.5, 1, 2, and 4 C, respectively. At the first 20 cycles (0.25 C), the capacity is not constant but decreases continuously. This behavior is consistent with the results shown in Figure 9. The reason behind this initial decrease is unknown and under investigation. The average capacity of the battery decreases from 1818 to 985 mAh g^{-1} with increasing *C*-rate from 0.25 C to 4 C. This rate capability is much better than that reported for corresponding carbon-silicon core–shell nanowires.[8,30] The capacity decreases from 1300 to 800 mAh g^{-1} with increasing *C*-rate from 0.2 to 1 C in[8] and from 2000 to ≈900 mAh g^{-1} with increasing *C*-rate from 0.1 to 2.5 C in Ref. [30]. The improved rate

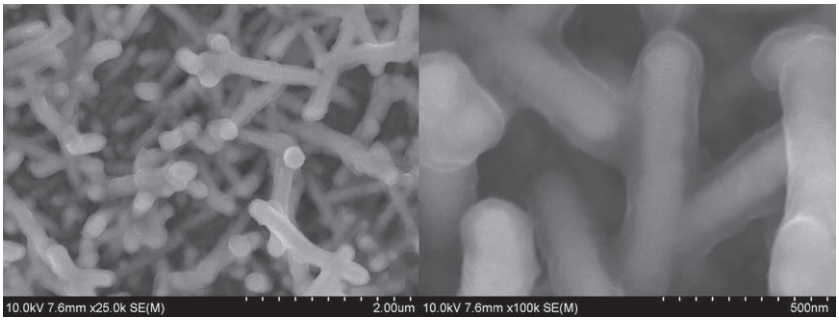

Figure 10. Silicon electrode structure after 70 cycles.

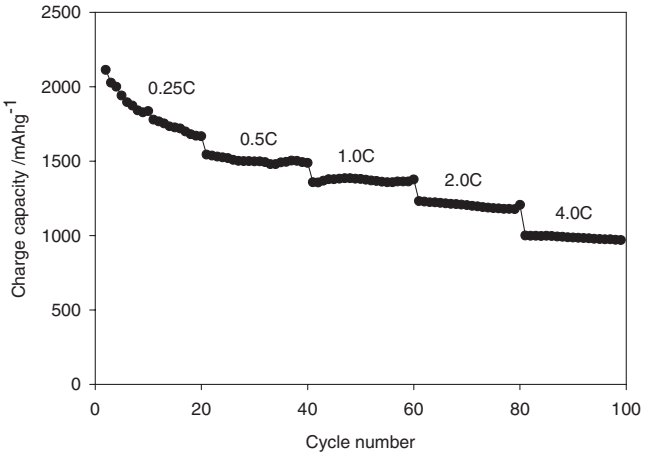

Figure 12. Rate performance of the electrodeposited silicon at various *C*-rates.

capability of our electrodeposited silicon anode can be attributed to the electronic conductivity of the nickel core within each silicon nanowire.[8,30]

3. Conclusions

A patterned 3D silicon anode was fabricated by electrodepositing silicon on a self-assembled TMV1cys-structured nickel current collector. Due to the integration of the nickel conductor within individual electrodeposited silicon nanowires and the uniform nature of the electrodeposited porous silicon coatings, the resulting high aspect ratio anode demonstrated significantly higher capacity (2300 mAh g^{-1}) than current graphite based anodes (372 mAh g^{-1}), as well as improved capacity retention (>1200 mAh g^{-1} at 173 cycles). Furthermore, the nanoscale thickness and large contact interface between the electrodeposited silicon coatings and the nickel core greatly enhanced rate performance. The charge capacity decreased only slightly from 1818 to 985 mAh g^{-1} with increasing *C*-rate from 0.25 to 4 C. The robust and stable TMV1cys/Ni/Si structure displays a high columbic efficiency (99.5%) and superior capacity retention (an average capacity decrease of only a 0.25% over the first 173 cycles). Finally, standard carbon coatings on the electrodeposited silicon greatly reduce the irreversible capacity to 22.5%. This novel anode architecture provides a simple and robust means to produce lithium-ion-based anodes with improved performance, stability, and rate capability.

4. Experimental Section

The detailed process for the fabrication of nickel-coated TMV1cys current collectors was given in our previous paper.[13]

Silicon electrodeposition on the TMV1cys/Ni current collector was performed in a three-electrode cell using a $SiCl_4$/PC (0.5 M, $SiCl_4$ 99.998%, PC 99.7% anhydrous, Sigma-Aldrich (MO, USA), use as received) as electrolyte with TBACl (0.1 M, Sigma-Aldrich 99%, dehydrated at 100 °C in vacuum before use) as a supporting electrolyte (Figure 3a). Platinum was used as counter and quasi-reference electrodes. Silicon was deposited at a constant voltage of –2.4 V (vs Pt QRE) on one side of a stainless steel disk where the TMV1cys/Ni was coated. The selection of a working voltage of –2.4 V was based on our and previous chronoamperogram, chronopotentiogram, and linear polarization measurements.[16,17,19] During the silicon electrodeposition, the total amount of consumed electrical charge was used to control the silicon deposition amount. Annealing and carbon coating were conducted in the glove box to reduce the irreversible capacity and stabilize the SEI film[19,27] of electrodeposited silicon. For annealing treatment, the prepared electrodeposited silicon samples were heated in an argon-protected furnace to remove impurities,[19] thereby decreasing the irreversible capacity. To realize the carbon coating, the samples were dipped into 8% polyacrylonitrile (PAN)/N-Methyl-2-pyrrolidone (NMP) solution. After being dried in a vacuum chamber in a glove box, the absorbed PAN was carbonized at 500 °C. The patterned 3D silicon anodes were characterized using a Hitachi (Tokyo, Japan) SU-70 HR-SEM with FFT images and a JEOL (Tokyo, Japan) 2100F field emission TEM. The Hitachi SU-70 HR-SEM with FFT images offers the ability to obtain EDS for elemental analysis of the samples.

The electrochemical performance of patterned silicon electrodes was tested in a coin cell using lithium metal as the counter electrode. The charge/discharge behaviors of silicon anodes were investigated using an Arbin (TX, USA) BT2000 workstation. The lithium insertion/extraction kinetics of silicon anodes was also characterized by electrochemical impedance spectroscopy and cyclic voltametry techniques using the solatron 1260/1287 electrochemical interface.

Acknowledgements

The authors acknowledge financial support from the Department of Energy (DESC0001160) under the project science of precision multifunctional nanostructures for electrical energy storage, Army Research Lab (W911NF1020078), National Science Foundation Nanomanufacturing Program (CMMI-0927693) and the Maryland Technology Development Corporation (TEDCO 09102380), as well as the technical support of the Maryland NanoCenter. J.N.C. also acknowledges the support of the Department of Energy, the Office of Basic Energy Sciences DEFG02–02-ER45975.

Received: July 20, 2010
Published online: November 9, 2010

[1] B. A. Boukamp, G. C. Lesh, R. A. Huggins, *J. Electrochem. Soc.* **1981**, *128*, 725.
[2] S. Cahen, R. Janot, L. Laffont-Dantras, J. M. Tarascon, *J. Electrochem. Soc.* **2008**, *155*, A512.
[3] U. Kasavajjula, C. Wang, A. J. Apple, *J. Power Sources* **2007**, *163*, 1003.
[4] C. K. Chan, H. Peng, G. Liu, K. McIlwrath, X. Zhang, R. A. Huggins, Y. Cui, *Nat. Nanotechnol.* **2008**, *3*, 31.
[5] C. K. Chan, R. Ruffo, S. S. Hong, R. A. Huggins, Y. Cui, *J. Power Sources* **2009**, *189*, 34.
[6] L. Cui, R. Ruffo, C. K. Chan, H. Peng, Y. Cui, *Nano Lett.* **2009**, *9*, 491.
[7] R. Ruffo, S. S. Hong, C. K. Chan, R. A. Huggins, Y. Cui, *J. Phys. Chem. C* **2009**, *113*, 11390.
[8] L. Cui, Y. Yang, C. Hsu, Y. Cui, *Nano Lett.* **2009**, *9*, 3370.
[9] H. Kim, J. Cho, *Nano Lett.* **2008**, *8*, 3688.
[10] K. Peng, J. Jie, W. Zhang, S. Lee, *Appl. Phys. Lett.* **2008**, *93*, 033105.
[11] M.-H. Park, M. G. Kim, J. Joo, K. Kim, J. Kim, S. Ahn, Y. Cui, J. Cho, *Nano Lett.* **2009**, *9*, 3844.
[12] T. Song, J. Xia, J. Lee, D. Hyun, M. Kwon, J. Choi, J. Wu, S. Doo, H. Chang, W. Park, D. Zang, H. Kim, Y. Huang, K. Hwang, J. Rogers, U. Paik, *Nano Lett.*, **2010**, *10*, 1710.

[13] X. Chen, K. Gerasopoulos, J. Guo, A. Brown, C. Wang, R. Ghodssi, J. N. Culver, *ACS Nano* **2010**, *4*, 5366.
[14] K. Agrawal, A. E. Austin, *J. Electrochem. Soc.* **1981**, *128*, 2292.
[15] C. H. Lee, F. A. Kröger, *J. Electrochem. Soc.* **1982**, *129*, 936.
[16] J. Gobet, H. Tannenberger, *J. Electrochem. Soc.* **1988**, *135*, 109.
[17] J. P. Nicholson, *J. Electrochem. Soc.* **2005**, *152*, C795.
[18] Y. Nishimura, Y. Fukunaka, *Electrochim. Acta* **2007**, *53*, 111.
[19] T. Munisamy, A. J. Bard, *Electrochim. Acta* **2010**, *55*, 3797.
[20] E. Royston, A. Ghosh, P. Kofinas, M. T. Harris, J. N. Culver, *Langmuir* **2008**, *24*, 906.
[21] K. Gerasopoulos, M. McCarthy, E. Royston, J. N. Culver, R. Ghodssi, *J. Micromech. Microeng.* **2008**, *18*, 104003.
[22] K. Gerasopoulos, M. McCarthy, P. Banerjee, X. Fan, J. N. Culver, R. Ghodssi, *Nanotechnology* **2010**, *21*, 055304.
[23] S. Lee, E. Royston, J. N. Culver, M. T. Harris, *Nanotechnology* **2005**, *16*, S435.
[24] K. T. Nam, D. W. Kim, P. J. Yoo, C. Y. Chiang, N. Meethong, P. T. Hammond, Y. M. Chiang, A. M. Belcher, *Science* **2006**, *312*, 885.
[25] J. P. Maranchi, A. F. Hepp, P. N. Kumta, *Electrochem. Solid-State Lett.* **2003**, *6*, A198.
[26] M. N. Obrovac, L. J. Krause, *J. Electrochem. Soc.*, **2007**, *154*, A103.
[27] J. Guo, X. Chen, C. Wang, *J. Mater. Chem.* **2010**, *20*, 5035.
[28] C. Wang, A. J. Appleby, F. E. Little, *J. Electroanal. Chem.* **2001**, *497*, 33.
[29] J. Wook Choi, J. McDonough, S. Jeong, J. Yoo, C. K. Chan, Yi Cui, *Nano Lett.* **2010**, *10*, 1409.
[30] W. Wang, P. N. Kumta, *ACS Nano* **2010**, *4*, 2233.